Applied Surface Science 258 (2012) 2169–2173

Contents lists available at ScienceDirect

Applied Surface Science

journal homepage: www.elsevier.com/locate/apsusc

Electrodeposition of Sb_2Se_3 on indium-doped tin oxides substrate: Nucleation and growth

Xuezhao Shi[a,b], Xin zhang[a], Yuan Tian[b], Chengmin Shen[b], Chunming Wang[a,*], Hong-Jun Gao[b,**]

[a] College of Chemistry and Engineering, Lanzhou University, Lanzhou 730000, China
[b] Institute of Physics, Chinese Academy of Sciences, Beijing 100190, China

ARTICLE INFO

Article history:
Available online 23 March 2011

Keywords:
Nucleation and growth
Antimony triselenide (Sb_2Se_3)
Electrodeposition
ITO antimony

ABSTRACT

The mechanisms related to the initial stages of the nucleation and growth of antimony selenide (Sb_2Se_3) semiconductor compounds onto the indium-doped tin oxides (ITO) coated glass surface have been investigated using chronoamperometry (CA) technique. The fabrication was conducted from nitric acid bath containing both Sb^{3+} and SeO_2 species at ambient conditions. No underpotential deposition (UPD) of antimony and selenium onto ITO substrate was observed in the investigated systems indicating a weak precursor–substrate interaction. Deposition of antimony and selenium onto ITO substrate occurred with large overvoltage through 3D nucleation and growth mechanism followed by diffusion limited growth. FE-SEM and XRD results show that orthorhombic phase Sb_2Se_3 particles with their size between 90 and 125 nm were obtained and the atomic ratio for antimony and selenium was 2:2.63 according to the EDX results.

© 2011 Elsevier B.V. All rights reserved.

1. Introduction

In recent several decades, V2–VI3 semiconductor compounds have attracted considerable attention because of their potential applications in thermoelectric power conversion devices, as well as in the fabrication of Hall Effect devices [1–3]. As a member of V2–VI3 semiconductor compound, Sb_2Se_3, a layer-structured direct band gap semiconductor with orthorhombic crystal structure, attracted much attention because of its excellent photovoltaic properties, photovoltaic properties and high thermoelectric power [1,2], which find applications for antimony triselenide in many fields, such as selective and decorative coating, optical and thermoelectric cooling devices [3].

Several methods have been used for preparing Sb_2Se_3 thin films on different substrates, chemical bath deposition [4–6], spray pyrolysis [7,8], radio frequency sputtering [9], and vacuum thermal evaporation [10–12], electrochemical from alkaline bath [13], acidic bath [14] and organic medium [15] etc. Electrochemical technologies have attracted much attention for preparing semiconductor thin films [16]. Compared with those capital-intensive physical methods, electrodeposition technique was a generally less expensive technique and had several advantages over dry processes such as the possibility for large-scale production of adherent and homogenous films, minimum waste of components, easy monitoring of the deposition process and conducted at ambient conditions. Therefore, electrodeposition method did not require expensive equipment (including vacuum plant), high temperature and lithography. The fabrication process was performed at ambient conditions and the possibility for diffusion of components and stress caused by temperature coefficient difference in the cooling process was avoided. Therefore, electrochemical method was a promising technique to produce semiconductor compounds.

However, few reports were reported on the nucleation and growth mechanism for fabrication of Sb_2Se_3 using electrochemical method. In this paper, current–time transients obtained by using chronoamperometry (CA) technique were used to investigate the nucleation and growth for electrodeposition of Sb_2Se_3 onto ITO substrate. The deposition potential was confirmed using CV techniques. Structure and surface morphology of the deposit were characterized by using X-ray diffraction (XRD) and field-emission scanning electron microscopy (FE-SEM).

2. Experiment

Electrochemical measurements were carried out on conventional homemade electrochemical cell with three-electrode system and the potentials were controlled by using a CHI 660A electrochemical workstation (USA). The ITO-coated glass (80 Ω/□) served as working electrode and was mounted to a small hole (0.3846 cm^2) at the bottom of the cell with its conductive side exposed to

* Corresponding author at: College of Chemistry and Engineering, Lanzhou University, Tianshui South Road 222#, Lanzhou 730000, China.
** Corresponding author at: Institute of Physics, Chinese Academy of Sciences, Zhongguancun South Three Street 8#, Beijing 100190, China.
E-mail addresses: cmwang@lzu.edu.cn (C. Wang), hjgao@iphy.ac.cn (H.-J. Gao).

0169-4332/$ – see front matter © 2011 Elsevier B.V. All rights reserved.
doi:10.1016/j.apsusc.2011.02.097

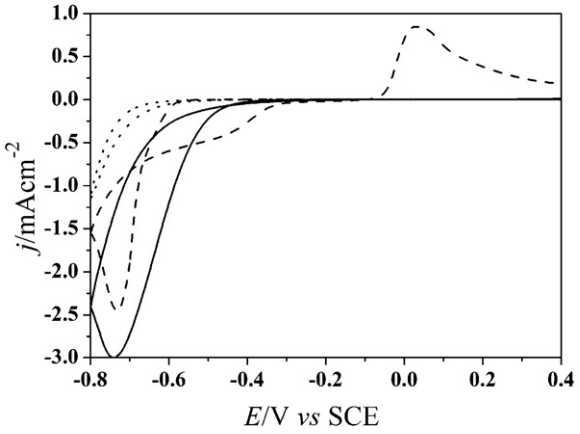

Fig. 1. Cyclic voltammograms for *n*-Si electrode recorded in different solutions: 0.1 M HNO_3 (dotted line); 4 mM Sb^{3+} + 0.1 M HNO_3 (dashed line); 2 mM SeO_2 + 0.1 M HNO_3 (solid line).

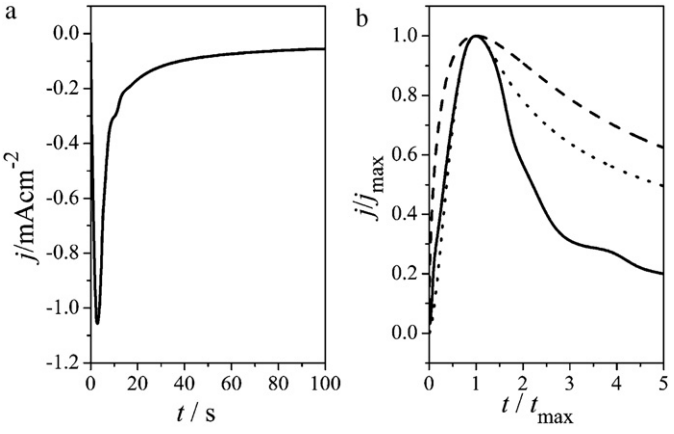

Fig. 2. (a) Current–time transient for selenium deposition onto ITO substrate at $E = -0.68$ V. (b) normalized current transient plotted in dimensionless form (solid line), the theoretical curve for instantaneous (dotted line) and progressive (solid line) nucleation.

solution. The counter electrode was a Pt wire and saturated calomel electrode (SCE) served as reference electrode. Previous to the electrochemical measurements, the ITO-coated glass was cut into small slices (1 cm × 1 cm). The small slices were rinsed ultrasonically with acetone and absolute ethanol for 15 min respectively, then rinsed with ultra pure water, and finally dried at 80 °C in air for use.

CV technique was used to investigate the electrochemical behavior of antimony and selenium on ITO substrates and confirm the deposition potential. CA technique was used to investigate the deposition mechanism and prepare the semiconductor compound. The deposition baths were as follows: 0.1 M HNO_3 + 2 mM SeO_2, 0.1 M HNO_3 + 4 mM Sb^{3+} and 0.1 M HNO_3 + 2 mM SeO_2 + 4 mM Sb^{3+}. All chemicals were of reagent grade and used without further purification. Milli-Q water (Millipore, 18.2 MΩ cm^{-1}) was used through all experiments. The crystalline structures of the deposited were identified by XRD (Rigaku D/max-2400, Cu *Kα* radiation, λ = 0.15406 nm). The morphology of the materials was studied by using FE-SEM (JSM-6380Lv Japan).

3. Result and discussion

3.1. Cathodic deposition of antimony and selenium onto ITO substrate from acidic solutions

As shown in the experimental section, electrochemical measurements of individual components onto ITO substrate were performed to investigate the formation mechanism of Sb_2Se_3 on ITO substrate. The deposition bath containing potassium antimony tartrate ($C_4H_4KO_7Sb/2H_2O$), SeO_2 and HNO_3 was utilized to investigate the optimum deposition potential for fabricating Sb_2Se_3 compounds.

In the background electrolyte (0.10 M HNO_3), a cathodic current appeared at the potential −0.60 V (dotted line in Fig. 1). This current should be attributed to the reduction of H^+, which occurred with an over voltage of 0.60 V. In reverse scan of the CV curve, no anodic currents appeared indicating that no oxidation process occurred on ITO substrate in blank solution. In the electrolyte containing 4 mM Sb^{3+} (dashed line in Fig. 1), the cathodic current began at the potential −0.60 V and a current peak appeared at $E = -0.72$ V. This current peak was caused by the reduction of Sb (III) on ITO electrode under diffusion limited process. On the reverse scan a narrow current hysteresis loop appeared in the potential range from −0.63 V to −0.3 V, similar to the electrochemical behavior of lead on silicon substrate [17]. This current hysteresis loop should be attributed to the self-catalyst property for reduction of antimony on the ITO electrode. That was to say, the reduction of antimony onto the predeposits was easier than that onto the bare ITO substrate. The reduction of antimony on ITO substrate occurred at the potential which was about 0.48 V negative to the equilibrium potential $E_{Sb\,(III)/Sb\,(0)} = -0.24$ V in contrast to that on gold substrate, which proceeded above the reversible potential [18,19]. This should be attributed to the formation of space charge region layer on the ITO substrate surface as well the low electrocatalytic activity of ITO towards reduction of Sb (III) species.

The reduction of antimony on ITO electrode surface occurred at potentials more negative than the equilibrium potential and no underpotential deposition of antimony was observed. Therefore, 2-dimensional (2D) deposition of antimony onto the ITO substrate was rule out and the deposition proceeded through 3D nucleation process on active sites and hemispherical diffusion towards the growing atom clusters. For better understanding the nucleation and growth kinetics of antimony in the electrodeposition process, current–time transients for deposition of antimony onto the ITO substrate were recorded at the constant potential $E = -0.60$ V. The corresponding curve was shown in Fig. 2a. In order to investigate the nucleation mechanism for antimony depositing onto ITO, the deposition transients were plotted in dimensionless form by normalizing two variables j and t with respect to the maximum current j_{max} and the corresponding time t_{max} at which point the maximum current was observed [20]. The theoretical plots for progressive and instantaneous nucleation growth mechanism were calculated according to following equations [21,22]:

$$\frac{i^2}{i_{max}^2} = 1.9542 \left[\frac{t_{max}}{t}\right] \left[1 - \exp\left(-1.2564 \frac{t}{t_{max}}\right)\right]^2$$

for instantaneous nucleation;

$$\frac{i^2}{i_{max}^2} = 1.2254 \left[\frac{t_{max}}{t}\right] \left[1 - \exp\left(-2.3367 \frac{t^2}{t_{max}^2}\right)\right]^2$$

for progressive nucleation. The calculated plots and the dimensionless form of experimental plot for reduction of antimony were presented Fig. 2b. Experimental deposition transient was in good agreement with the theoretical curve for instantaneous nucleation and growth mechanism before maximum value, after which the experimental deposition transient decreased rapidly deviating the instantaneous process. The deviation might be caused by partial kinetic control of the growth [23].

On the reverse scan, at the potential positive to 0.02 V the voltammograms presented the anodic current for stripping of antimony. The separation between anodic and cathodic current peak

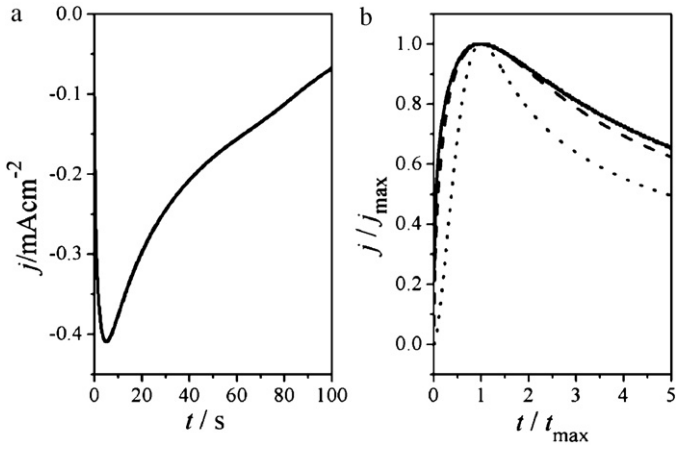

Fig. 3. (a) Current–time transient for selenium deposition onto ITO substrate at $E = -0.60$ V. (b) normalized current transient plotted in dimensionless form (solid line), the theoretical curve for instantaneous (broken line) and progressive (solid line) nucleation.

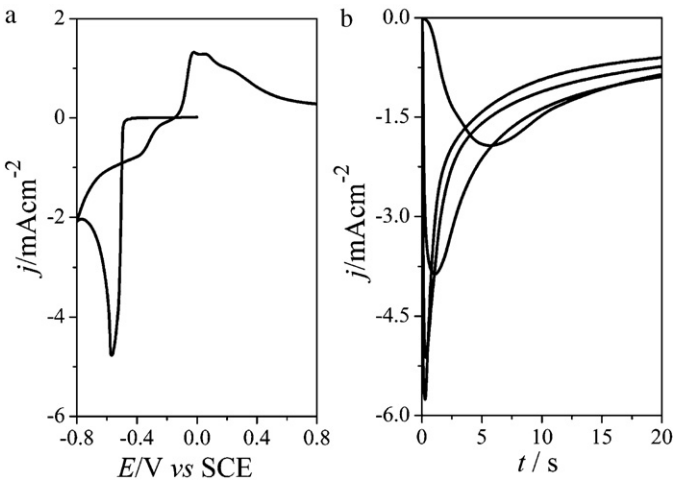

Fig. 4. (a) Cyclic voltammograms and (b) current–time curves at different potentials recorded on ITO electrode in 4 mM Sb^{3+} + 2 mM SeO_2 + 0.1 M HNO_3.

was 0.74 V, which was much larger than $2.3RT/nF$ (or $59/n$ mV at 25 °C) [24] which was the character for a reversible Nernst reaction, indicating that the deposition of antimony onto ITO substrate was an irreversible process.

In the solution containing 2 mM SeO_2 the cathodic current appeared at $E < -0.42$ V (solid line in Fig. 1) resulting from reduction of Se (IV) on the ITO substrate. The reduction of Se on ITO substrate began at the potential about 0.72 V negative of the equilibrium potential $E_{Se(IV)/Se(0)} = +0.30$ V in contrast to the reversible potential [25,26], indicating low electrocatalytic activity for ITO substrate. The current for the reduction of Se (IV) onto ITO substrate was characterized by a peak at $E = -0.74$ V at the forward potential scan, which was typical for nucleation followed by diffusion limited growth. The reverse scan shows a current hysteresis loop (not obvious in the CV curve) in the potential range from −0.45 to 0 V, indicating the autocatalytic Se (IV) reduction. The current hysteresis loop and the absence of UPD for Se onto ITO excluded low dimensional nucleation and phase formation process and presented a weak deposit–substrate (Se–ITO) interaction. No anodic current for oxidation of Se was observed in the potential range should be attributed to the formation of a barrier on ITO/Se interface [27].

Similar to antimony, current–time transients for deposition of Se were also recorded at the potential −0.60 V. The corresponding curve was presented in Fig. 3a. Theoretical plots for 3D progressive and instantaneous nucleation growth process and the dimensionless form of experimental plot were shown in Fig. 3b. The dimensionless form of experimental deposition transient was in good agreement with the curve for progressive nucleation mechanism in the whole deposition process, indicating that the reduction of Se onto ITO substrate proceeded following progressive 3D nucleation and growth mechanism.

3.2. Electrochemical fabrication of Sb_2Se_3 compounds onto ITO electrode

In 0.10 M nitric acid solution containing 4 mM Sb^{3+} and 2 mM SeO_2 the onset current occurred at potential −0.42 V (Fig. 2a). Compared with that in background electrolyte only containing SeO_2 or Sb^{3+}, this cathodic current should be attributed to the reduction of Se (IV) because the reduction of Sb^{3+} occurred at more negative potential. However, the cathodic current peak shift positively to −0.58 V compared to that of SeO_2 and the current intensity also increased. These changes should result from the influence of Sb (III). The strong interaction between Se (IV) and Sb (III) would make the deposition potential shift positively [28,29]. As the potential scanned negatively, the reduction of antimony occurred and the sharp cathodic current increase should be attributed to the codeposition of Sb and Se. On the reverse scan, a broad anodic current peak with two shoulder peaks appeared at about −0.01 V. This anodic current should be attributed to the stripping of antimony from the deposits and the shoulder peak may result from the presence of Se in the deposits. Nevertheless, the two shoulder peaks should not be caused by stripping of Se because no Faraday process occurred in this potential region for ITO substrate in the solution only containing Se (IV) species.

Fig. 4b presented the current density–time transients recorded at different constant potentials −0.52, −0.54, −0.56 and −0.58 V in stationary electrolyte. The current density–time transients presented that the cathodic current reached its maximum value at the very initial stages of the deposition (0.2–5 s) and then decreased to a nearly constant value with the increase of time. Additionally, both the maximum current and the time needed to reach the maximum current depended on the applied potential: the more negative was the potential, the higher was the maximum current and the shorter time was needed to reach the maximum current.

The morphology image of the deposits obtained at $E = -0.54$ V recorded by SEM was shown in Fig. 5a. According to the SEM image, uniform particles with diameter at about 90–125 nm was obtained on the substrate. The EDX analysis showed that the element ratio for Sb:Se was 2: 2.65 in the deposit, a little larger than the stoichiometry value (2:3). The crystalline structure was investigated using X-ray dispersion (XRD) and the XRD pattern of the deposits was shown in Fig. 5b. The deposit presented a preferred (2 1 0) orientation based on standard card (JCPDS, 72-1184), indicating that the deposits were abundant in (2 1 0) facets, and thus their (2 1 0) planes tended to be preferentially oriented parallel to the substrate surface [30]. The experimental peak indicated that orthorhombic phase Sb_2Se_3 compound was fabricated by electrochemical method. A broad peak appeared between 15 and 30° should be attributed to the amorphous glass.

Since the potential for fabrication of Sb_2Se_3 ($E = -0.54$ V) compound was not sufficient for reduction of antimony, Se particles formed in the over potential region according to the following equation:

$$H_2SeO_3 + 4e^- + 4H^+ \rightarrow Se + 3H_2O \quad (1)$$

which was the first stage of Sb_2Se_3 formation on the ITO substrate. When Se particles formed on the ITO substrate, the

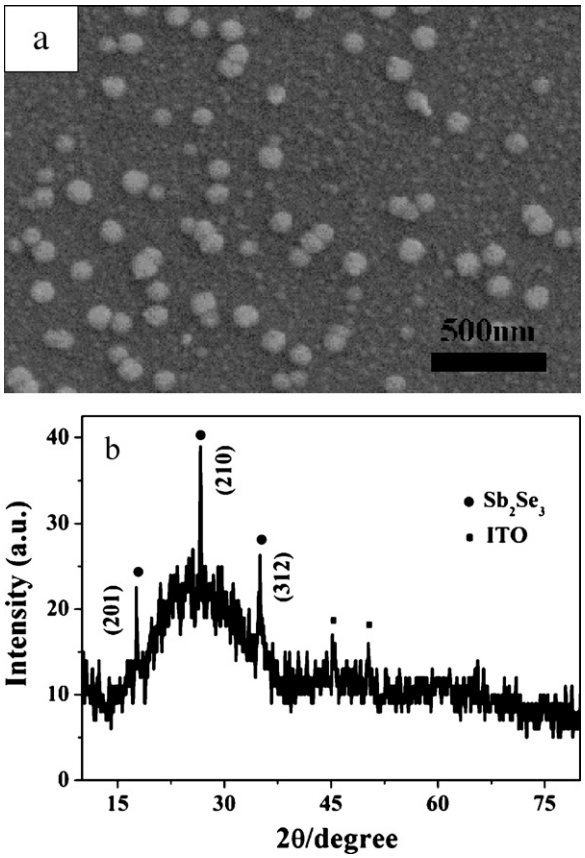

Fig. 5. (a) SEM image and XRD pattern (b) for Sb_2Se_3 electrodeposited onto ITO at $E = -0.54$ V.

deposition of Sb^{3+} occurred on the surface of Se particles because of the strong interaction existed between Se particles and soluble Sb (III) species, accompanying the formation of Sb_2Se_3 compound:

$$3Se + 2Sb^{3+} + 6e^- \rightarrow Sb_2Se_3 \quad (2)$$

Further growth of Sb_2Se_3 onto ITO substrate completed by alternate deposition of Se onto the Sb_2Se_3 particles and antimony onto the surface of Se and Sb_2Se_3, and finally formed bulk Sb_2Se_3 compounds.

3.3. Electrochemical behavior of ITO/Se and ITO/Sb_2Se_3 electrodes in solution containing Sb^{3+}

Fig. 6 (solid line) presented the voltammograms for Se coated ITO electrode in 0.1 M HNO_3 solutions containing 4 mM Sb^{3+}. In the forward potential scan, the cathodic current caused by the reduction of antimony onto ITO/Se began at −0.46 V, forming a small current peak at −0.51 V, caused by reduction of antimony onto the surface of Se clusters. Compared to that on ITO substrate, the peak potential shift positively which should be caused by the stronger interaction between predeposited Se and Sb (III) [28,29] than that between ITO substrate and Sb (III). As the potential scanned negatively, the cathodic current increased again and a stronger current peak was observed at the potential −0.6 V. This current peak should result from bulk deposition of antimony. On reverse potential scan, the anodic current was occurred at the potential $E = 0.00$ V. This current was caused by the stripping of antimony rather than Se because no oxidation of Se occurred in this potential range.

The voltammogram for ITO/Sb_2Se_3 electrode in 4 mM Sb^{3+} + 0.1 M HNO_3 recorded under ambient conditions was shown in Fig. 7 (solid line). In this case, the reverse scan was

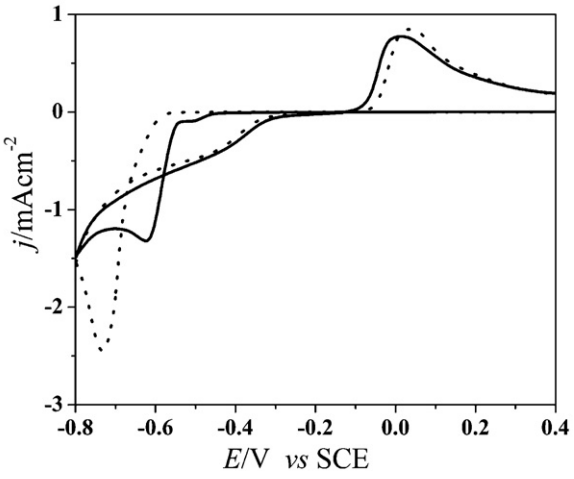

Fig. 6. Cyclic voltammograms for ITO/Se electrode in 4 mM Sb^{3+} + 0.1 M HNO_3 (solid line) and the ITO electrode in 4 mM Sb^{3+} + 0.1 M HNO_3 (dashed line).

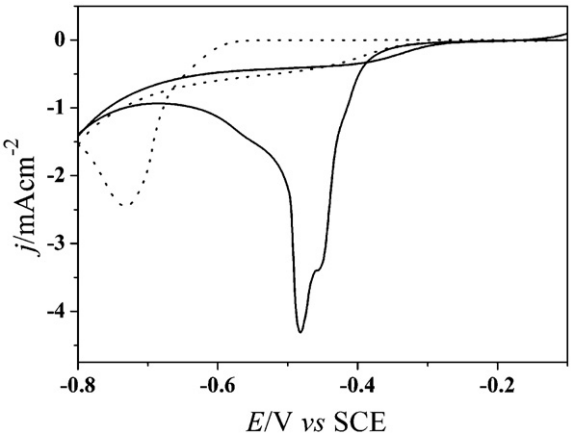

Fig. 7. Cyclic voltammograms for ITO/Sb_2Se_3 (solid line) and ITO (dashed line) electrode in 4 mM Sb^{3+} + 0.1 M HNO_3 recorded under ambient conditions.

stopped at 0.0 V to prevent the preformed Sb_2Se_3 compound from being destroyed. In the forward scan, the electrochemical behavior for antimony onto Sb_2Se_3 was similar to that onto ITO/Se substrate. The cathodic current began at potential −0.30 V, positive to that onto ITO and ITO/Se substrate, indicating a stronger interaction between Sb_2Se_3 and antimony. The shoulder peak at potential −0.45 V should attribute to the deposition of antimony onto surface of Sb_2Se_3 particles. While as the potential scanned negatively, the current peak appeared at about −0.48 V should be attributed to the bulk deposition of antimony on both Sb_2Se_3 particles and on the partially exposed ITO substrate.

4. Conclusion

The deposition of antimony and Se onto ITO coated glass occurred with large overvoltage and was characterized by 3D nucleation and growth mechanism followed by diffusion controlled process. The potential for the fabrication of Sb_2Se_3 was more negative than equilibrium potential for the reduction of Sb^{3+} and Se(IV) indicating the deposition of Sb_2Se_3 onto ITO coated glass was an irreversible process. The mechanism of Sb_2Se_3 nucleation onto ITO coated glass includes OPD of 3D islands of Se followed by deposition of antimony onto surface of Se particles. The further Sb_2Se_3 growth was accomplished by codeposition of antimony (deposition onto Se and Sb_2Se_3) and Se (OPD onto antimony and Sb_2Se_3).

Acknowledgments

The work is supported by the Special Doctoral Foundation of the Ministry Education of China (Grant No. 20775030) and National Natural Science Foundation of China (Grant No. 50872147), 863 Program (Grant No. 2007AA03Z305).

References

[1] J. Black, E.M. Conwell, L. Sigle, C.W. Spencer, J. Phys. Chem. Solids 2 (1957) 240–251.
[2] N.S. Platakis, H.C. Gatos, Phys. Status. Solidi. A Appl. Res. 13 (1972) K1–K4.
[3] K.Y. Rajapure, C.D. Lokhande, C.H. Bhosele, Thin Solid Films 311 (1997) 114–118.
[4] I. Grozdanov, Semicond. Sci. Technol. 9 (1994) 1234–1241.
[5] Y. Rodriguez-Lazcano, Y. Pena, M.T.S. Nair, P.K. Nair, Thin Solid Films 493 (2005) 77–82.
[6] R.S. Mane, C.D. Lokhande, Mater. Chem. Phys. 82 (2003) 347–354.
[7] C.H. Bhosale, M.D. Uplane, P.S. Patil, C.D. Lockhande, Thin Solid Films 248 (1994) 137–139.
[8] S.R. Gadakh, C.H. Bhosale, Mater. Chem. Phys. 78 (2002) 367–371.
[9] M.Y. Versavel, J.A. Haber, Thin Solid Films 515 (2007) 7171–7176.
[10] P. Arun, A.G. Vedeshwar, Thin Solid Films 335 (1998) 270–278.
[11] P. Kumar, R. Thangaraj, Solid State Commun. 140 (2006) 525–528.
[12] A.G. Vedeshwar, J. Phys. III France 5 (1995) 1161–1172.
[13] J.D. Desai, K.N. Ganage, Bull. Electrochem. 15 (1999) 318–320.
[14] A.P. Torane, K.Y. Rajpure, C.H. Bhosale, Mater. Chem. Phys. 61 (1999) 219–222.
[15] A.P. Torane, C.H. Bhosale, J. Phys. Chem. Solids 63 (2002) 1849–1855.
[16] D. Lincot, Thin Solid Films 487 (2005) 40–48.
[17] B. Rashkova, B. Guel, R.T. Pötzschke, G. Staikov, Electrochim. Acta 43 (1998) 3021–3028.
[18] C.M. Wang, Y.L. Du, Z.L. Zhou, Electroanalysis 14 (2002) 849–852.
[19] J.W. Yan, Q. Wu, W.H. Shang, B.W. Mao, Electrochem. Commun. 6 (2004) 843–848.
[20] R. Krumm, B. Guel, C. Schmitz, G. Staikov, Electrochim. Acta 45 (2000) 3255–3262.
[21] G. Gunagardena, G. Hills, I. Montenegro, B. Scharifker:, J. Elactroanal. Chem. 138 (1982) 225.
[22] B. Scharifker, G. Hills:, Electrochim. Acta 28 (1983) 879.
[23] S.B. Sadale, P.S. Patil, Solid State Ionics 167 (2004) 273–283.
[24] A.J. Bard, L.R. Faulkner, in: H. David (Ed.), Electrochemical Methods: Fundamentals and Applications, second ed., John Wiley & Sons, Inc., 2001, pp. 239–243.
[25] M.O. Solaliendres, A. Manzoli, G.R. Salazar-Banda, K.I.B. Eguiluz, S.T. Tanimoto, S.A.S. Machado, J. Solid State Electrochem. 12 (2008) 679–686.
[26] M. Alanyalioglu, U. Demir, C. Shannon, J. Electroanal. Chem. 561 (2004) 21–27.
[27] Y.A. Ivanova, D.K. Ivanou, E.A. Streltsov, Electrochem. Commun. 9 (2007) 599–604.
[28] X.Z. Shi, X. Zhang, C.L. Ma, C.M. Wang, J. Solid State Electrochem. 14 (2010) 93–99.
[29] J.Y. Yang, W. Zhu, X.H. Gao, S.Q. Bao, X. Fan, X.K. Duan, J. Hou J. Phys. Chem. B 110 (2006) 4599–4604.
[30] Y.G. Sun, Y.N. Xia, Science 298 (2002) 2176–2179.